

AUTHOR QUERIES

AUTHOR PLEASE ANSWER ALL QUERIES

PLEASE NOTE: Please note that we cannot accept new source files as corrections for your article. If possible, please annotate the PDF proof we have sent you with your corrections and upload it via the Author Gateway. Alternatively, you may send us your corrections in list format. You may also upload revised graphics via the Author Gateway.

Carefully check the page proofs (and coordinate with all authors); additional changes or updates WILL NOT be accepted after the article is published online/print in its final form. Please check author names and affiliations, funding, as well as the overall article for any errors prior to sending in your author proof corrections. Your article has been peer reviewed, accepted as final, and sent in to IEEE. No text changes have been made to the main part of the article as dictated by the editorial level of service for your publication.

- AQ:1 = Please confirm whether the edits made in the current affiliation of all the authors are correct.
- AQ:2 = Please confirm or add details for any funding or financial support for the research of this article.
- AQ:3 = Please provide the expansions of the acronyms FCT/MCTES, EU, COST, CA, INTERACT, SNF, and BID/ICI-FE for your funding agency. Providing the correct acknowledgment will ensure proper credit to the funder.
- AQ:4 = If you haven't done so already, please make sure you have submitted a graphical abstract for your paper. The GA should be a current figure or image from your accepted article. The GA will be displayed on your articles abstract page on IEEE Xplore. Please choose a current figure from the paper and supply a caption at your earliest convenience for the graphical abstract. Note that captions cannot exceed 1800 characters (including spaces). If you submitted a video as your graphical abstract, please make sure there is an overlay image and caption. Overlay images are usually a screenshot of your video that best represents the video. This is for readers who may not have access to video-viewing software. Please see an example in the link below: <http://ieeaccess.ieee.org/submitting-an-article/>

Received 21 March 2024, accepted 30 April 2024. Date of publication 00 xxxx 0000, date of current version 00 xxxx 0000.

Digital Object Identifier 10.1109/ACCESS.2024.3399602

Service Quality of the Urban Microcellular Scenario in the Sub-6 GHz Frequency Bands

RUI R. PAULO¹, (Member, IEEE), EMANUEL B. TEIXEIRA, (Member, IEEE),
AND FERNANDO J. VELEZ¹, (Senior Member, IEEE)

Departamento de Engenharia Eletromecânica (DEM), Faculdade de Engenharia, Instituto de Telecomunicações, Universidade da Beira Interior, 6201-001 Covilhã, Portugal

Corresponding author: Rui R. Paulo (rrp@lx.it.pt)

This work was supported in part by FCT/MCTES through National Funds co-funded by EU funds under Project UIDB/50008/2020 and Project UI/BD/150923/2021, in part by COST CA 20120 INTERACT, in part by ORCIP under Grant 22141-01/SAICT/2016, in part by SNF Scientific Exchange—AISpectrum under Project 205842, in part by European Union's Horizon 2020 Research and Innovation Program under the Marie Skłodowska-Curie Project through TeamUp5G under Grant 813391, and in part BID/ICI-FE/Santander Universidades-UBI/2016-17 Scholarship.

ABSTRACT This paper compares the service quality between 4G and 5G New Radio (NR) among different sub-6 GHz frequency bands in an urban micro-cellular outdoor setting. An updated version of LTE-Sim is considered to obtain the exponential effective signal-to-interference-plus-noise ratio in 4G while determining the modulation and coding scheme. System capacity is obtained by considering a video application at 3.1 Mb/s and the proportional fair (PF) scheduler while comparing 4G and 5G NR through system-level simulations (the 5G-air-simulator is considered for 5G NR). The modified largest weighted delay first (M-LWDF) scheduler is compared with the PF, though only in 4G. Optimal system performance is reached both in 4G and 5G NR for cell radii longer than two times the breakpoint distance (or beyond), which are preferable compared to the shortest values for the cell radius. We have learned that the packet loss ratio (PLR) is higher for the cell radii, R , shorter than breakpoint distance, d'_{BP} . For $d'_{BP} \leq R \leq 1000$ m, the PLR first decreases and then increases. For a target PLR $< 2\%$, in 4G, the highest maximum average goodput is obtained with the M-LWDF scheduler (10-25% increase). This maximum occurs at the 2.6 GHz and 3.5 GHz frequency bands for $300 \leq R \leq 500$ m, while at 5.62 GHz the highest goodput occurs for the longest R s. With 5G NR and the PF, the maximum average goodput increases, in our simulations, from ≈ 14.1 (in 4G) to 26.1 Mb/s (20 MHz bandwidth).

INDEX TERMS 5G-air-simulator, exponential effective SINR mapping, ITU-R M.2135-1, LTE-Sim, modulation and coding scheme, small cell networks, sub-6 GHz frequency bands, two-slope model, urban micro cell scenario.

I. INTRODUCTION

The exponential growth of the wireless communications sector has driven the research community to investigate future systems, such as heterogeneous networks (HetNets), millimeter-wave and multi-input multi-output [1], [2], [3]. To complement the traditional macro-cell network to answer future service demands and the growth of wireless data traffic [4], [5], [6], lower power nodes are being added to the

The associate editor coordinating the review of this manuscript and approving it for publication was Yafei Hou¹.

existing networks, creating what is known as HetNets. The effectiveness of the answer to HetNets business opportunities is determined by the diversity of cell sizes and network architectures, in combination with the coalition of diverse technologies and availability of licensed and unlicensed frequency bands.

A. SINGLE VS. DUAL-SLOPE PATH LOSS MODELS

Studies on the performance analysis of cellular networks usually consider single-slope (SS) path loss models (PLMs).

SS are simple PLMs that fail to capture the short-distance path loss behavior [7]. This happens since an SS-PLM considers a homogeneous path loss along the cell coverage range, as shown in Fig. 1.

Investigate the efficiency of resource allocation in LTE-Advanced and 5G New Radio (NR) networks using precise system-level simulations.

In urban deployment scenarios, where there are a plethora of non-homogeneous obstacles, such as vehicles and urban obstructions and elements, attenuation increases when the distance between the transmitter and the receiver nodes increases. This may lead to inaccurate results in the performance evaluation of dense networks. Dual-slope (DS) PLMs can be a solution to overcome the limitations of SS-PLMs since these models more accurately represent the outdoor small cell link variations along the distance (represented by the change in the propagation exponent beyond the breakpoint distance), mainly due to the combination of a direct ray, including a ray reflected on the ground (e.g., asphalt).

DS-PLMs represent the dependence of the path loss over distance, which implies a DS behavior [8]. The authors from [9] have shown that, compared to SS-PLMs, DS-PLMs more closely matches empirical data while capturing the relationship between the path loss and the distance between the transmitter and the receiver. While the propagation exponent slope is approximately 2-2.2 for distances in the range close to the cell center, a value of approximately 4 is identified for the longest distances, as shown in Fig. 1b. According to [10], the breakpoint distance can be obtained either by regression analysis or by considering the geometry when the Fresnel zone just touches the ground. The breakpoint distance can also define the turning point between the line-of-sight (LoS) and non-line-of-sight (NLoS) situations, as explained in [8] and [10]. Furthermore, PLMs can be generalized for any number of slopes, as in [11].

B. RELATED WORK

DS-PLMs have captured the attention of the research community for decades, and are being studied in a multitude of verticals. One of these areas is vehicular technology in applications, such as intravehicular [12], [13], vehicle-to-vehicle [14], [15], vehicle-to-cyclist [16], vehicle-to-infrastructure [17] or pedestrian-to-vehicle [18] communications. Another area of application is unmanned aerial vehicles (commonly known as UAVs) operating at a low altitude [19]. Some deployment scenarios are also being considered for rural [3], [15], highway [15], suburban [3] or urban [20] environments, where a detailed analysis has been conducted to consider street canyon environments [21] or indoor scenarios [22], [23]. Coverage in these scenarios is provided by cells with a longer cell radius, R , known as macro-cells. However, the cell radius of indoor and urban small cells is shorter [11], [24], [25].

Furthermore, millimeter wavebands are considered to answer the enormous amount of information demand in small cell networks [26]. However, although DS-PLMs have been considered only SS-PLMs are applied, as the breakpoint distance is far beyond the size of small cells. The literature review contains research works on frequency bands from 800 MHz up to 82.5 GHz [27], [28], [29]. Current research studies are being carried out in urban areas utilizing millimeter waves, as in [29].

Although several propagation scenarios have been considered and developed for 5G [30], the underlying impact of different packet scheduling algorithms is still being investigated [31]. For successive generations of broadband cellular networks, packet scheduling has played an important role in managing radio resources. In particular, aiming at providing a user quality of service (QoS) that guarantees a sufficient grade of service, the choice of the packet scheduler is of particular interest.

QoS metrics are network-centric performance variables that do not directly consider the user experience. Usually, QoS metrics may be based on four key quantitative parameters: packet loss ratio (PLR), throughput (or goodput), packet delay and jitter [32]. Indirectly, these QoS metrics may be mapped into quality of experience [33].

Packet schedulers have been developed to support real-time (RT) services, such as videoconferencing, or non-real-time (NRT) services, such as internet browsing [34], [35]. In 4G, there are two key strategies for downlink (DL) packet scheduling: the QoS-aware and QoS-unaware strategies [36]. Prior to this classification, DL scheduling strategies have also been divided into channel-dependent and channel-sensitive strategies [35].

The authors from [25] and [37] evaluated the impact of the different path loss models on the capacity of 4G networks composed of small cells considering a carrier frequency of 2.6 GHz. They compared four urban path loss models, two SS-PLMs, one DS-PLM in LoS, and another DS-PLM, for NLoS. They concluded that for values of R longer than the breakpoint, the supported cell physical throughput is steady or decreases with R when using the traditional SS propagation models. In addition, for values of R shorter than the breakpoint, the two-slope propagation model leads to values of the throughput lower than those obtained with the SS-PLMs.

The 2.6 GHz, 3.5 GHz and 5.62 GHz sub-6 GHz frequency bands were studied in [38]. With mathematical modeling, the authors from [38] concluded that, in terms of a supported throughput, for R when shorter than ≈ 550 m, the 2.6 GHz frequency band presents the highest throughput. For cell radii of $550 \lesssim R \lesssim 690$ m, the 3.5 GHz frequency band presents the highest throughput. For cell radii longer than ≈ 690 m, the 5.62 GHz frequency band is the best one.

C. URBAN MICRO CELLULAR SCENARIO

In this study, differently from [39], where only a modeling approach was followed, the small cell performance is

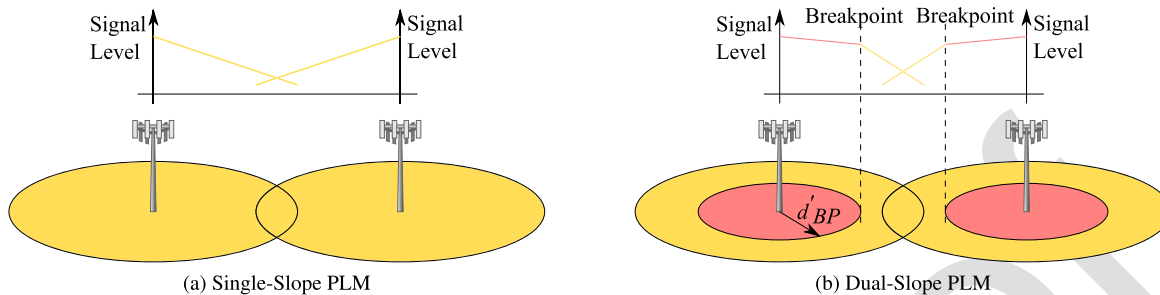


FIGURE 1. Different slope behaviors in the path loss models of the cellular system.

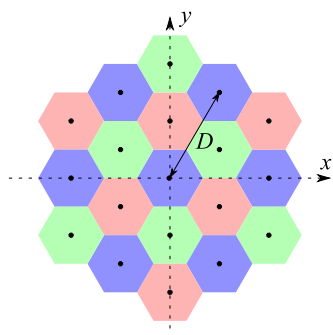


FIGURE 2. Simulation scenario for the UMi LoS small cell network with reuse pattern three. There is a tier of interference with the same number of subchannels in each node.

evaluated through system level simulations by first applying an improved version of LTE-Sim [40]. LTE-Sim is an open-source framework that simulates LTE-Advanced networks, which was improved earlier to produce the results presented in [33] and [41]. Then, in an effort to replicate the results for 5G, the expected differences of the presented study considering LTE-Sim in relation to those using the 5G New Radio (5G NR) simulator (the 5G-air-simulator), from the University of Bari, are identified [42]. Similarities and improvements in the frequency reuse trade-off and its impact on service quality and underlying system capacity boundaries are analyzed.

In this work, the urban micro cellular (UMi) scenario for LoS, defined by ITU, in [43], and a given reuse pattern have been included in LTE-Sim. In addition, the supported throughput is also analytically studied based on the average signal-to-interference-plus-noise ratio (SINR), while comparing analytical and simulation results for the system capacity achieved when $PLR < 2\%$ in deployments either with video application only or with video plus best effort usage. Fig. 2 presents the frequency reuse for the considered small cell deployment, where D is the reuse distance.

An outdoor environment is considered where the antennas of the BS and the user equipment (UE) are well below the tops of the surrounding buildings. Nineteen small cells are deployed with frequency reuse pattern three. The impact of varying the cell radius is analyzed.

This UMi cell deployment scenario is presented in [43], with a focus on pedestrian and slow vehicular users. We have considered that the radio link between the cell nodes and the UEs is in LoS. The DS-PLM is considered to determine coverage and cochannel interference.

D. CONTRIBUTIONS

The first contribution of this work consists of investigating the relation between physical throughput and the size of the cells. This analysis is achieved using an implicit function formulation. We explore how the supported throughput varies on average among different frequency bands within the sub-6 GHz range concerning the coverage distance R , as elaborated in [39]

As the average SINR and the average exponential effective SINR mapping (EESM) present a trend similar to the supported throughput curve, we aim at identifying optimal values for R where these parameters are simultaneously maximized through system level simulations for different frequency bands. Particularly, we have extracted average EESM results and their cumulative distribution function (CDF) at the UE for different values of the cell radius.

One explores the MCS supported by different users inside the cell, whose results are expressed in terms of the CDF of the MCS and their performance characteristics. We examine the performance of resource management in LTE-Advanced and 5G NR networks through accurate system-level simulations.

Whilst comparing the performance differences between 4G and 5G NR networks, assuming the Proportional Fair (PF) packet scheduler, we consider the 3rd Generation Partnership Project (3GPP) technical specification (TS) 22.105 [44]. This specification defines performance targets for the PLR of video streams when users employ continuous video communication in the downlink direction. One compares the impact of using the PF and M-LWDF schedulers. As a novelty, the M-LWDF scheduler is a QoS-aware scheduler capable of distinguishing different service types. Our evaluation encompasses to determine several performance metrics, such as average PLR, goodput and delay. Furthermore, we also evaluate the maximum average goodput and the number of supported users in the air interface, taking into account video

and best effort (BE) applications. Particularly, BE packets are transmitted only when sufficient resources are available, as in [33].

In summary, the main contributions of this work can be summarized as follows:

- 1) Verification of the system capacity (goodput, number of supported users) through an event-driven simulation approach and system quality evaluation (PLR, delay) of small cells modeled by the UMi DS path loss models in 4G and 5G networks;
- 2) Detailed analysis of the impact of considering different packet schedulers for video applications;
- 3) Update of the LTE-Sim and 5G-air-simulators with truly uniform distributions of users, and obtaining surface charts of the spatial behavior of EESM and MCS.

The remainder of the paper is organized as follows. Section II presents the generalized single and the ITU-R M.2135-1 dual slope path loss model. In Section III, the considered schedulers are addressed. Section IV describes the simulation scenario. The cellular planning trade-off is presented in Section V, where results for the EESM, the achieved MCS and the supported cell throughput are presented. The achievable system performance for PLR < 2% (and maximum delay less than the 150 ms target) is studied in Section VI. From the results of the PLR, the goodput, and the delay as a function of the maximum number of users, the system capacity is determined in terms of the supported goodput considering the PF in 4G and 5G NR. The performance improvement of considering the M-LWDF scheduler is studied in Section VII, though only for 4G. Finally, conclusions are drawn in Section VIII, where suggestions for further research are also presented. Table 1 provides the mathematical notations used throughout the paper.

II. PATH LOSS MODELS

Signal transmission is subject to propagation loss or path loss. The diversity and the types of obstacles between the transmitter and the receiver (such as buildings, trees, vehicles, and lampposts) have a substantial contribution to the accounting of the total propagation losses. Cellular optimization trade-offs result from the co-channel interference imposed by nodes in the same heterogeneous network layer or by nodes in other sub-layers operating with the same sub-channels.

The cellular planning process allows the prediction of the cell range, cell coverage and throughput trade-offs [7], [20], [45], [46]. In the cellular optimization and planning process, propagation losses are expressed through SS-PLMs and DS-PLMs.

A. SINGLE SLOPE MODELING

For the sake of simplicity, let us consider the PLMs presented in [2], [8], and [47], a generalization of other SS-PLMs studied in [25] and [28]. Apart from the constant parameters,

TABLE 1. Mathematical notation.

| Symbol | Description |
|--------------|---|
| α_0 | reference loss, at one meter |
| α_i | factor computed from the QoS for the i_{th} user |
| β | estimated parameter that results from link-level simulations |
| γ | propagation exponent |
| δ_i | acceptable PLR for the i_{th} user |
| τ_i | delay threshold for the i_{th} user |
| c | velocity of the RF signal in free space |
| C | carrier |
| d | distance between the BS and the receiver |
| d_{BP} | breakpoint distance |
| D | distance between two cells operating with the same set of subchannels |
| $D_{HOL,i}$ | head of line (HOL) delay for the i_{th} user |
| f_c | frequency |
| h_{BS} | antenna heights for the BSs |
| h_{UE} | antenna heights for the UEs |
| I | interference |
| k | frequency reuse pattern |
| σ | vector of the individual values of the SINR for each subcarrier |
| r_{ij} | throughput achieved by the i^{th} user on the j^{th} subchannel |
| r_{cc} | reuse factor |
| R | cell radius |
| R_b | throughput (bit rate) |
| \bar{R}_i | average throughput for the i^{th} ring |
| R_{b_sup} | supported cell throughput |
| w_{ij} | priority metric for the i^{th} user on the j^{th} subchannel |

the path loss, PL , only depends on the distance between the BS and the receiver, d . The generalized equation for a SS-PLM, PL_1 , is defined as follows:

$$PL_1 = \alpha_0 d^\gamma, \quad (1)$$

α_0 is the reference loss, at one meter, and γ is the propagation exponent (which, in this case, is constant for any value of d), while d takes any value between one meter and R . The propagation exponent could be determined experimentally by using an interpolation procedure [22].

SS-PLMs are the simplest way to model propagation losses since they have simple mathematical expressions and may lead to a large error between the PLM and the local path loss values [7]. Because of their “single” mathematical expression, SS-PLMs do not capture the impact of different topographic environments, the difference in the behavior after the distance that separates the zone where the first Fresnel zone just touches the ground, or even the impact of irregular cell patterns [7]. In HetNets, SS-PLMs also fail to estimate losses since the laws of physics applied to urban environments where there is a reflection on the ground,

which shows that a dual slope (DS) behavior is observed. This behavior is more evident in small cell networks for the sub-6 GHz bands [48]. To overcome the above limitations of the SS-PLM, the DS-PLM can be used since they can appropriately describe the channel propagation behavior in the UMi scenario.

B. URBAN MICRO LINE-OF-SIGHT DUAL SLOPE MODELING

We considered the UMi scenario in LoS and the deterministic DS-PLM from [43]. Eq. 2 presents the path loss, between the BS, at the cell center, and UEs located up to the breakpoint distance, PL_a , as shown in Fig. 1b.

$$PL_a = 22.0 \log_{10}(d) + 28.0 + 20 \log_{10}(f_c), \quad (2)$$

where d is in meters and f_c is the frequency given in GHz. For distances longer than the breakpoint distance, PL_b , is calculated by Eq. 3 as follows:

$$PL_b = 40.0 \log_{10}(d) + 7.8 - 18 \log_{10}(h_{BS} - 1.0) - 18 \log_{10}(h_{UE} - 1.0) + 2 \log_{10}(f_c), \quad (3)$$

where h_{BS} and h_{UE} are the antenna heights for the BSs and UEs, respectively. The BS and UE antennas are outdoors and located below the rooftops of the surrounding buildings.

The breakpoint distance, d'_{BP} , is computed as follows:

$$d'_{BP} = \frac{4(h_{BS} - 1.0)(h_{UE} - 1.0)f_c}{c}, \quad (4)$$

where c is the velocity of the RF signal in free space (equal to the speed of light), generally accepted to be approximately 3×10^8 m/s. d'_{BP} is either determined when the first Fresnel zone just touches the ground or by the turning point between the LoS and NLoS zones [4], [10].

The authors from [25], [39], [48], and [49] compare mathematical modeling approaches between SS-PLMs and DS-PLMs. They show that the use of DS-PLMs implies higher supported throughput for the longest cell radii in small-cell outdoor environments. The authors from [4], [11], and [48] highlight that DS-PLMs present more accurate performance results for coverage probability and user association than SS-PLMs. In fact, DS-PLMs are gaining importance in the characterization of propagation environments of successive generations of mobile communications systems in earlier 3GPP releases [30] and in 5G NR scenarios [31], [50]. In [50], the 2D distance is replaced by the 3D distance in PL_a and PL_b . While the PL_a equation remains the same, PL_b is different, as presented in [51].

III. PACKET SCHEDULING

Packet scheduling occurs at the BS, as shown in Fig. 3. In its simple form, the scheduler receives the information about the desired QoS and system configuration, as well as the channel quality indicator (CQI) determined by the UE. After gathering this information, the eNB, responsible for

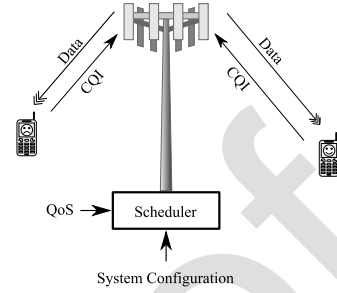


FIGURE 3. Simplified view of the scheduler operation.

distributing the available radio resources among UEs decides on the assignment of resource blocks (RBs) for the UEs and how many RBs should be assigned to transport the data [52].

In recent years, DL packet schedulers have been studied to maximize the end-user QoS [36]. As mentioned before, QoS considers a network centric approach and evaluates several performance parameters of broadband cellular networks, such as PLR, goodput and delay. The choice of the most efficient packet scheduling algorithm was studied in [31] and [36].

As a QoS-unaware scheduler, PF does not consider any QoS parameter [35], [52], [53]. It only schedules the traffic from a user when its instantaneous channel quality is high compared to its own average channel conditions over time. The priority metric is defined as follows:

$$w_{ij} = \frac{r_{ij}}{\bar{R}_i}, \quad (5)$$

where w_{ij} is the priority metric for the i^{th} user on the j^{th} subchannel, r_{ij} is the throughput achieved by the i^{th} user on the j^{th} subchannel and \bar{R}_i is the average throughput achieved by the i^{th} user [32].

As a QoS-aware scheduler [35], [52], M-LWDF extends the metric considered in PF by taking factors, such as delay and PLR, into consideration as follows:

$$w_{ij} = \alpha_i D_{HOL,i} \frac{r_{ij}}{\bar{R}_i}, \quad (6)$$

where α_i is a factor computed from the QoS and $D_{HOL,i}$ is the head of line (HOL) delay for the i_{th} user. The factor α_i is determined as follows:

$$\alpha_i = -\frac{\log(\delta_i)}{\tau_i}, \quad (7)$$

where δ_i is the acceptable PLR for the i_{th} user and τ_i is the delay threshold for the i_{th} user [32].

While the strength of the PF is the good trade-off between the system throughput and the data rate fairness among users, its weakness is the low achieved spectral efficiency. In turn, M-LWDF is an inefficient scheduler at overloaded considerations but allows supporting considerable system throughput while enabling an acceptable level of fairness [35].

TABLE 2. Radio Parameters for the 4G and 5G NR Networks.

| Parameters | Frequency Bands | | |
|--|-----------------|----------------|-----------------|
| | 2.6 GHz n7 | 3.5 GHz n78 | 5.62 GHz n46 |
| Transmitter power of small cells [dBm] | 40 | 42.2478 | 46.6953 |
| Transmitter power of UT [dBm] | 23 | | |
| Number of BS | 19 | | |
| Reuse pattern | 3 | | |
| Bandwidth per tier [MHz] | 20 | | |
| Effective BS height [m] | 10 | | |
| Effective UT height [m] | 1.5 | | |
| Cell radius [m] | [20, 1000] | | |
| Packet scheduler | PF, M-LWDF | | |
| TTI [ms] | 1 | | |
| 5G NR numerology μ | 0 | | |
| 5G NR subcarrier spacing [kHz] | 15 | | |
| 5G NR no. of subframes per radio frame | 10 | | |
| 5G NR no. of slots per sub-frame | 1 | | |
| 5G NR no. of slots | 10 | | |
| 5G NR no. of symbols per slot | 14 | | |
| 5G NR radio frame duration [ms] | 10 | | |

IV. UMI TEST SCENARIO

A. PHYSICAL REUSE SCENARIO

According to [43], the UMi test scenario is composed of nineteen small cells with frequency reuse pattern three ($k = 3$), as presented in Fig. 2. This scenario deployment is an outdoor environment with a high density of users and traffic loads, where the antennas of the BSs and UEs are well below the rooftops.

The results have been extracted at the central hexagonal-shaped cell, while interference is imposed by the six cochannel cells in the first tier of interference, as shown in Fig. 2. When users move to another cell, they struggle with handover and start using the subchannels from the frequency band available in the new cell. The inter-site distance, D , is the distance between two cells operating with the same set of subchannels and is equal to $D = \sqrt{3}kR$, where R is the cell radius [37].

B. RADIO AND SIMULATION PARAMETERS

This work compares the 4G and 5G NR radio coverage and frequency reuse trade-off for the 2.6 GHz, 3.5 GHz, and 5.62 GHz frequency bands, the operative bands n7, n78, n46, respectively. As n7 and n46 bands are being used by mobile operators, performance is compared as presented in [54] and [55]. The PF and the M-LWDF are then compared

considering only 4G. The bandwidth available per tier is 20 MHz, i.e., 60 MHz bandwidth in total, as reuse pattern three is considered. In Fig. 2 the cell of interest is the center cell, and the six cells from the first tier of interference, filled in the blue color. Different frequencies are represented by different colors in Fig. 2. The height of the small cell BS is 10 meters, while the height of the UE is 1.5 meters. R varies from 20 m up to 1000 m. Table 2 presents the values of the radio parameters.

Improvements in the LTE-Sim and 5G-air-simulator were made to account for the UMi scenario. The versions of the LTE-Sim simulator and 5G-air-simulator considered in this work includes not only the improvements specifically implemented for this work, e.g., facilitating to obtain surface charts for EESM and MCS, but also previous improvements, which are freely available under the GPLv3 license in [56] and [57]. Although the 5G-air simulator already considers fast fading, the 4G LTE-Sim did not consider it. In both simulators, the LoS scenario is addressed.

For comparison purposes, while the LTE-Sim has been used to simulate the 4G network, its successor (the 5G-air-simulator) has been considered for 5G NR (with numerology 0 and 20 MHz bandwidth). Numerology 0 is considered for 5G non-stand alone, as it compares to 4G. The improvements from LTE-Sim to 5G-air-simulator have involved upgrading the bandwidth manager class in the code of the simulator (to accommodate the 3.5 GHz and 5.62 GHz frequency bands for the DL and uplink). The class that defines the location of the cells has also been updated to consider a frequency reuse of three, as shown in Fig. 2.

V. CELLULAR PLANNING TRADE-OFF

The carrier-to-interference ratio (C/I) and SINR are considered in the cellular planning in the DL while assuming orthogonal frequency division multiplexing with a static allocation scheme. The adoption of dynamic MCSs entails that each MCS corresponds to a minimum value of the SINR. Coverage and frequency reuse optimization is required to optimize the radio and network planning trade-off.

A. CARRIER-TO-INTERFERENCE RATIO FORMULATION

C/I is composed of a formulation with exact values of the interference from the BS of the first, second, and third tiers of cochannel cells (interfering nodes) into the UEs placed at the edge of the cell, which can be expressed Eqs. 8, 9, 10, as shown at the bottom of the next page, [25]. In these equations, the exact position of each interferer is considered in each tier of interference. In the DL, C/I is given by the Eqs. 8, 9 and 10 for the 1st, 2nd and 3rd rings of interference of the small cell network, while the reuse pattern is $k = 3$ [25], [39].

Considering the first tier of interference is a valid approximation for propagation exponent 4, since the interference obtained from the second and third tiers is minimal compared to the preceding tiers. However, for propagation exponent 2, at least the second tier of interference needs to be considered in the simulations, N.B.: in Eqs. 8, 9, 10, one does not

TABLE 3. Values of the breakpoint distance for different frequency bands.

| Parameters | Frequency Bands | | |
|---------------|-----------------|----------------|-----------------|
| | 2.6 GHz n7 | 3.5 GHz n78 | 5.62 GHz n46 |
| d'_{BP} [m] | 156 | 210 | 337.2 |

represent different propagation exponents, although different distances are considered for R and D , and different exponents may then be applied in the real computations.

B. SIGNAL-TO-INTERFERENCE-PLUS-NOISE RATIO ALONG THE CELL

Figs. 4a and 4b present the variation in the SINR along with the distance from the cell center to the UE d for the cell coverage radii of $R = 100$ m and $R = 500$ m, where $0 \leq d \leq R$. The behavior of the SINR curve is similar for the curves of all frequency bands. The noise power is added to the interference power. Eq. 8, is considered to compute the distances of the six interference BSs (at the first ring of interference) to the UE at the edge of the central cell, in the worst case. A minor inflection point is observed at corresponding to the breakpoint distance. The breakpoint distance is calculated by considering Eq. 4. Values of the breakpoint distance are presented in Table 3.

The 2.6 GHz frequency band shows the highest SINR. Due to the highest path loss between the small eNB and the UEs when the C/I is lower, the resulting SINR is lower. In practice, this effect is more evident near the cell edge because, overall, the chance of having NLoS at long distances is higher. The propagation exponent is $\gamma = 2.2$ for the shortest d s, which corresponds to a considerably lower SINR, as shown in Fig. 4a and Fig. 4b.

C. SUPPORTED CELL THROUGHPUT

The supported cell throughput can be used as a measure to predict the system capacity. By considering the implicit function formulation from [39], the supported cell throughput is computed by weighting the physical throughput at each coverage ring according to the size of the crown as follows:

$$R_{b_sup} = \sum_{i=1}^n \frac{R_{b_i}(d_i^2 - d_{i-1}^2)}{R^2}, \quad (11)$$

where R_{b_i} is the physical throughput for the MCS that corresponds to the i^{th} ring, d_i is the distance associated with the i^{th} ring/crown [39]. The mapping between SINR and the throughput (R_b) considered in the LTE-Sim and the 5G-air-simulator is presented in Table 4.

Theoretical results for the supported throughput are presented in Fig. 5, where the mapping with the average SINR [39] is also presented. For the considered frequency bands, for cell radii shorter than 1000 m, the values of the supported throughput per cell, R_{b_sup} , are similar among the bands for R s up to circa d'_{BP}/r_{cc} , where r_{cc} is the reuse factor (for example, at 2.6 GHz, $d'_{BP} = 156$ m, then $R = 52$ m for $k = 3$, and $r_{cc} = \sqrt{3k} = 3$). For R s shorter than this value, the propagation exponent for interference is $\gamma = 2.2$. Only for $D = r_{cc} \times R$ beyond d'_{BP} does the propagation exponent become $\gamma = 4$, and the system capacity benefits from the highest power decay. Then, it increases faster for the lowest frequency bands but achieves a similar maximum value. For R s up to approximately 877 m, even though lower values of the supported throughput occur at 5.62 GHz, one can perceive that when the system becomes noise limited (not interference limited anymore), the supported throughput at 5.62 GHz becomes higher than those at 2.6 GHz and 3.5 GHz (for R s of approximately 960 m and 877 m, respectively). After achieving its maximum values of 38.7 Mb/s, 38.5 Mb/s and 38.2 Mb/s for the 2.6 GHz, 3.5 GHz and 5.62 GHz frequency bands, the supported throughput decreases at 610 m, 815 m or 1040 m (although the latter results are not shown in the viewed graph) for 2.6 GHz, 3.5 GHz and 5.62 GHz.

D. EXPONENTIAL EFFECTIVE SINR MAPPING

In its simplified way, the SINR measured by the UE in the DL is a ratio between the desired signal and the unwanted sum of noise and interference. The SINR of a subcarrier can be calculated as a function of the subcarrier power [44]. At the system level, exponential effective SINR mapping (EESM) combines multiple SINR values from multiple subcarriers into an effective SINR function [44], [58], [59]. EESM is mapped to a value of CQI and is a method that maps all subcarriers of a user that uses the same MCS. The main overall idea of EESM is to compress the SINR values from each subcarrier into a single value that represents channel conditions.

For LTE-Advanced, in this work, we consider a bandwidth of 20 MHz, yielding the availability of 100 sub-channels,

$$\frac{C}{I}_{1st} = \frac{R^{-\gamma}}{2(D + 0.66394R)^{-\gamma} + 2(D - 0.31395R)^{-\gamma} + (D + R)^{-\gamma} + (D - R)^{-\gamma}}, \quad (8)$$

$$\frac{C}{I}_{2nd} = \frac{R^{-\gamma}}{2(\sqrt{3}D + 0.88915R)^{-\gamma} + 2(\sqrt{3}D + 0.8591R)^{-\gamma} + 2(\sqrt{3}D - 0.84799R)^{-\gamma}}, \quad (9)$$

$$\frac{C}{I}_{3rd} = \frac{R^{-\gamma}}{2(2D + 0.55802R)^{-\gamma} + 2(2D + 0.47727R)^{-\gamma} + (2D + R)^{-\gamma} + (2D - R)^{-\gamma}}. \quad (10)$$

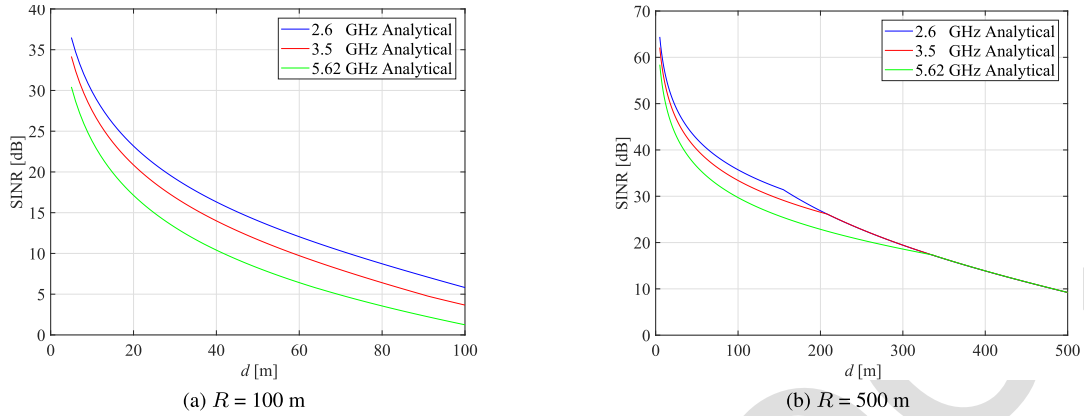


FIGURE 4. Comparison of the SINR among 2.6, 3.5 and 5.62 GHz frequency bands.

TABLE 4. LTE-Sim and 5G-air-simulator Mappings into the Physical throughput for 20 MHz bandwidth.

| CQI | 4G | | | | | 5G NR | | | | |
|-----|-----------|-----------|------------------|------|--------------|-----------|-----------|------------------|------|--------------|
| | SINR [dB] | MCS Index | Modulation Order | ITBS | R_b [Mbps] | SINR [dB] | MCS Index | Modulation Order | ITBS | R_b [Mbps] |
| 1 | -4.63 | 0 | 2 | 0 | 2.797 | -6.75 | 0 | 2 | 0 | 3.589 |
| 2 | -2.6 | 2 | 2 | 2 | 4.584 | -4.96 | 1 | 2 | 2 | 5.773 |
| 3 | -0.12 | 4 | 2 | 4 | 7.224 | -2.96 | 3 | 2 | 5 | 11.337 |
| 4 | -2.26 | 6 | 2 | 6 | 10.296 | -1.01 | 5 | 2 | 7 | 15.734 |
| 5 | 4.73 | 8 | 2 | 8 | 14.112 | 0.96 | 7 | 2 | 8 | 18.007 |
| 6 | 7.53 | 10 | 2 | 9 | 15.84 | 2.88 | 9 | 2 | 9 | 20.310 |
| 7 | 8.67 | 12 | 4 | 11 | 19.848 | 4.92 | 11 | 4 | 11 | 25.964 |
| 8 | 11.32 | 14 | 4 | 13 | 25.456 | 6.7 | 13 | 4 | 14 | 36.851 |
| 9 | 14.24 | 16 | 4 | 15 | 30.576 | 8.72 | 15 | 4 | 15 | 39.364 |
| 10 | 15.21 | 18 | 4 | 16 | 32.856 | 10.51 | 18 | 6 | 17 | 46.393 |
| 11 | 18.63 | 20 | 6 | 18 | 39.232 | 12.45 | 20 | 6 | 18 | 50.880 |
| 12 | 21.32 | 22 | 6 | 20 | 46.888 | 14.35 | 22 | 6 | 21 | 64.520 |
| 13 | 23.47 | 24 | 6 | 22 | 55.056 | 16.07 | 24 | 6 | 23 | 73.763 |
| 14 | 28.49 | 26 | 6 | 24 | 61.664 | 17.88 | 26 | 6 | 25 | 81.659 |
| 15 | 34.6 | 28 | 6 | 26 | 75.376 | 19.97 | 28 | 6 | 26 | 85.069 |

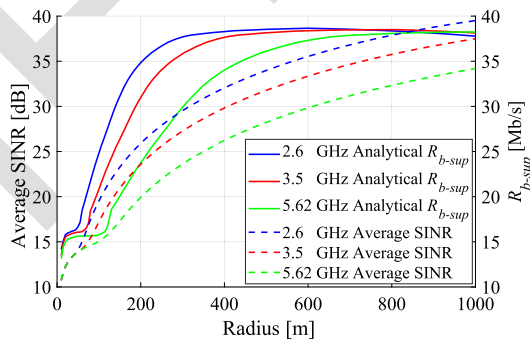


FIGURE 5. Mapping between the average SINR and the equivalent supported throughput for the 2.6, 3.5 and 5.62 GHz frequency bands for values with a cell radius of up to 1000 m.

into a single value that expresses the channel conditions, the following EESM equation is considered [44], [58]:

$$EESM(\sigma, \beta) = -\beta \ln \left(\frac{1}{N} \sum_{i=1}^N e^{-\frac{\sigma_i}{\beta}} \right), \quad (12)$$

σ is the vector of the individual values of the SINR for each subcarrier, with individual components σ_i . The values of β are an estimated parameter that results from link-level simulations and are determined case-by-case for different MCSs [60]. These values of β are obtained from curves generated by considering additive white Gaussian noise for each value of MCS [58]. LTE-Sim is used to determine the EESM, whilst considering $\beta = 1$, and Eq. 12 becomes an exponential weight of all SINR values.

Fig. 6 presents high-resolution results for the EESM considering cell radii of 100 m and 500 m. Figs. 6a, 6b and 6c present the results for the cell radius of 100 m for the three

which then results in 100 different values of SINR. At the UE, a value of SINR is calculated for each subcarrier for each TTI ($= 1$ ms). To combine $N = 100$ different values of SINR

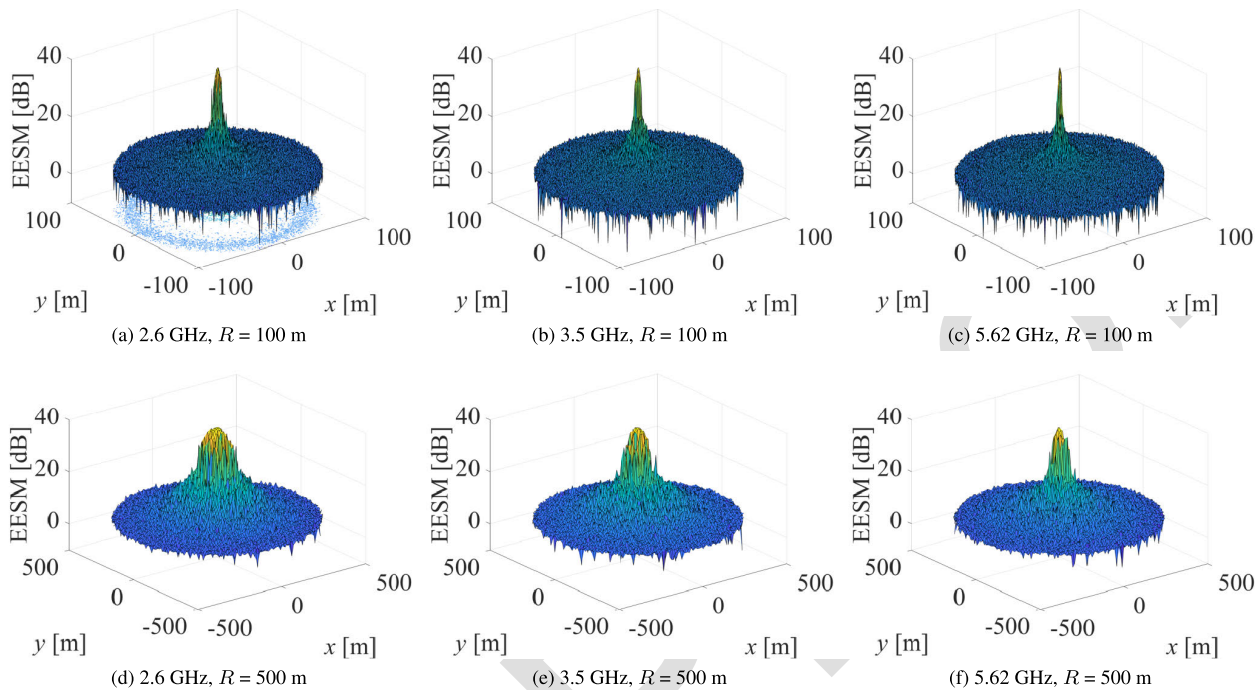


FIGURE 6. EESM for cell radii of 100 m and 500 m.

frequency bands. A short cell radius implies low values for the EESM, especially near the cell edge. This occurs since the interference imposed by the interfering neighboring cells is too high.

Fig. 6a presents the results for the lowest considered frequency, i.e., 2.6 GHz, where there is a slight advantage compared to the other two frequency bands. In the 2.6 GHz band, the highest values of EESM occur for a broader zone of the total area of the cell compared to the other two bands, and then in the 3.5 GHz frequency band, compared to the 5.62 GHz band, as shown in Fig. 6b. When the cell radius varies from 100 m to 500 m (Figs. 6d, 6e and 6f), there is a clear enhancement in the EESM, which achieves the highest values in a broader central zone of the cell. The increase in frequency leads to a similar behavior in comparison with cells of 100 m. The 5G-air-simulator considers the mutual information effective SINR mapping (MIESM) method [42] instead of ESSM, whose basis is the formulation presented in [61].

Fig. 7 presents the results for the cumulative distribution function (CDF) of EESM for radii of 100 m and 500 m and a bandwidth of 20 MHz. For $R = 100$ m and an EESM up 8 dB, the 2.6 GHz frequency band achieves 93%, for 3.5 GHz the frequency band achieves 95% and for 5.62 GHz the frequency band achieves 97%. By considering $R = 500$ m, EESM equal to 8 is used in 72% of the cell area for the 2.6 GHz and 3.5 GHz frequency bands, while the corresponding area is 76% for cells operating at the 5.62 GHz band.

E. ACHIEVABLE MODULATION AND CODING SCHEME

UEs determine the CQI from the value of EESM from the received transmission. After the determination of the CQI, the UE sends its value to the cell node via a feedback

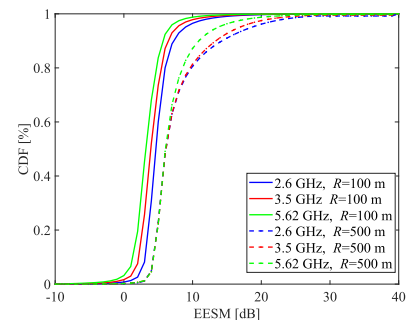


FIGURE 7. Comparison of the CDF of the EESM between different frequency bands for the cell radii of 100 m and 500 m.

channel with the adjustable delay. With this received channel quality information, the cell node can determine the MCS and translate it to the transport block size (TBS) with an adequate procedure [52]. The MAC sublayer determines the payload for the physical layer. This payload is the TBS and quantifies the number of bits to be transferred in the ongoing TTI (1 ms). The TBS table available from [62] provides the amount of data to be transmitted to the UE.

Fig. 8 presents the results of the CDF as a function of the MCS (a discrete variable) for $R = 100$ m and 500 m. At 2.6 GHz for $R = 100$ m, 86% of the packets achieved an MCSs lower than 10, while in the 3.5 GHz and 5.62 GHz frequency bands MCSs lower than 10 are achieved by 90% and 95% of the packets, respectively.

When $R = 500$ m, the values of the MCSs are identical for the 2.6 GHz and 3.5 GHz frequency bands. In these bands, 69% of the packets achieved an MCS lower than 12, whereas

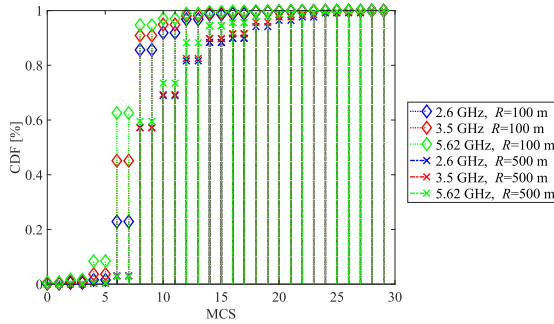


FIGURE 8. Comparison of the CDF of the MCSs among different frequency bands for the cell radii of 100 m and 500 m.

for the 5.62 GHz frequency band, 73% of the packets achieve an MCS lower than 12.

VI. SIMULATION RESULTS FOR THE PF SCHEDULER AT THE SATURATION LEVEL

The results for system capacity are determined at a saturation level corresponding to PLR < 2% (and maximum delay less than the 150 ms target), according to 3GPP TS 22.105 [44]. The PLR is the ratio between the total number of packets that do not reach their destination and the total transmitted packets. Above this 2% threshold, the user’s service quality (mapped into the quality of experience) decays. The network topology considered in this work and presented in Fig. 2 is composed of a set of small cell nodes and UEs. UEs are uniformly assumed to be distributed in the central cell, according to the assumptions from [33]. Results for PLR, goodput, delay, and number of supported users for 4G were obtained with LTE-Sim and for 5G with 5G-air-simulator.

A. SIMULATION METHODOLOGY

For 4G and 5G NR, simulations ran for different values of R and frequency bands by initially considering only one user. To obtain the statistical significance of the results, each combination of the parameters was simulated 100 times. First, we extracted values for the average PLR. If the average PLR did not surpass the 2% threshold (for video flows), we would add one more user and perform 100 new simulation runs for each R (represented in kilometers) and the frequency band. Then, users kept being added up to the PLR and surpassed the 2% threshold. For the sake of readability, not all the simulated number of users are presented in the view charts. A 95% confidence interval has also been considered.

More simulation parameters need to be considered to evaluate the radio network performance, as presented in Table 5. The considered application is a video with a bit rate of 3.1 Mb/s [63], one of the video traces made available in the simulators by us [56], [57] to represent higher bit rate applications, as before only video traces up to 440 kb/s bit rate were available. Other video traces can be added by the researcher community in a tailored way. The simulated time is 46 seconds, and video flows have a duration of 40 seconds.

TABLE 5. Simulation Parameters for the 4G and the 5G NR Networks.

| Parameters | Frequency Bands | | |
|-------------------------|-----------------|----------------|-----------------|
| | 2.6 GHz n7 | 3.5 GHz n78 | 5.62 GHz n46 |
| Application | Video | | |
| Bit rate [Mb/s] | 3.1 | | |
| Simulation duration [s] | 46 | | |
| Flows duration [s] | 40 | | |
| Number of simulations | 100 | | |

B. PACKET LOSS RATIO

In this Section, we go beyond the performance results for 4G networks, with the PF scheduler, by considering the 5G-air-simulator (for 5G NR). Our contribution to the 5G-air-simulator was including the UMi_A LoS path loss model (with 3D distance [51]). Figs. 9 and 10 present results for the average PLR as a function of R , with the number of users as a parameter, (varying from one up to fifteen, for 4G, and from one to twenty-seven, for 5G NR), by considering the above mentioned approach (only results for more than six users are shown for 4G, and for more than seventeen for 5G). The impact of the variation of the results after the breakpoint distance can be observed for all frequency bands. For values of R that are shorter than the breakpoint distance, the PLR is considerably higher (with increasing values for the shortest R s) and presents the worst results.

In Fig. 10, the results for the PF scheduler and the 5G NR are shown. The results show the same behavior as for 4G (Fig. 10). For cell radii shorter than d'_{BP} , the PLR increases when R s become shorter. For the longest R s, the PLR also increases. Lower values for the PLR are obtained for cell radii slightly longer than d'_{BP} . In 5G NR, as PLR decreases compared to 4G NR, the number of supported users increases.

C. SYSTEM CAPACITY

The maximum average goodput is also determined considering the PLR threshold of 2% by using the results achieved with the LTE-Sim (4G) and the 5G-air-simulator while considering a video (VID) application. The maximum average goodput is extracted for all the considered frequency bands, as shown in Fig. 11 (where the analytically supported throughput is determined by considering Eq. 11, and represented as a solid line). For 4G, considering the PF scheduler (in dotted line), the maximum average goodput is 14.11 Mb/s, 14.07 Mb/s and 12.64 Mb/s for the frequency bands of 2.6 GHz, 3.5 GHz and 5.62 GHz and for R of 300 m, $R = 400$ m and $R = 300$ m, respectively. Because the system becomes noise limited for the longest cell radii, for all frequency bands, there is a decrease in the average goodput after its maximum is achieved.

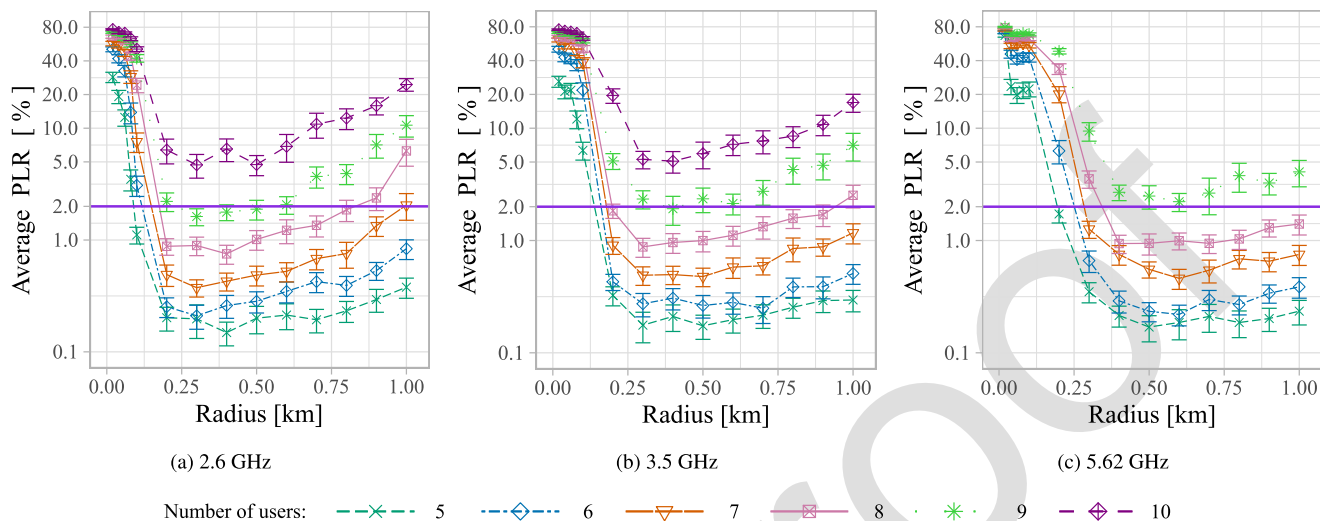


FIGURE 9. 4G results for the average PLR as a function of the cell radius with the number of users as a parameter for the different frequency bands for the PF scheduler and 3.1 Mb/s video trace.

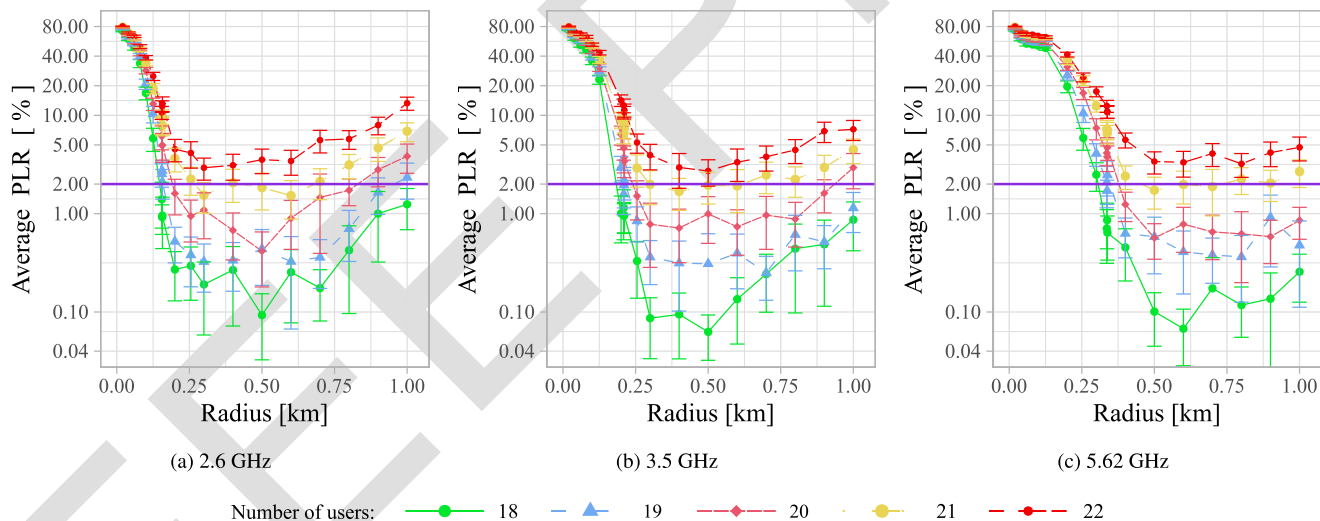


FIGURE 10. 5G NR results for the average PLR as a function of the cell radius with the number of users as a parameter for the different frequency bands for the PF scheduler and 3.1 Mb/s video trace.

As it is important to compare the quality of service of 5G networks that use the same frequencies and assume the same bandwidth (20 MHz), a cellular network with the same topology and similar radio system parameters was considered in system level simulations performed with the 5G-air-simulator while assuming numerology 0, and only considering the PF scheduler. Assumptions for the 5G NR simulation parameters are presented in Table 2 and Table 5.

When 5G NR is considered, for the PF scheduler and the video application, the maximum average goodput increases up to 26.1 Mb/s starting in values of R from 300 m, 400 m and 500 m for the 2.6 GHz, 3.5 GHz and 5.62 GHz bands, respectively, as shown in Fig. 11b. In these simulation results, the 95% confidence interval does not exceed 0.2% of the represented value.

Fig. 11b presents the maximum analytical supported throughput for 5G NR. The maximum analytically supported throughput increases for values ≈ 38.5 Mb/s (in 4G) of up to values of approximately 76 Mb/s for the three considered frequency bands. By only considering the video application, with an average bit rate of 3.1 Mb/s, it can be observed that values much lower than the maximum analytically supported throughput are achieved.

To make use of the resources that may still be available, it can be considered that, apart from watching video, users also consume BE applications. The BE application is modeled as an ideal greedy source that always has packets to send; it only transmits packets when there are available resources to send them [33]. The lines identified with "VID+BE" in the view chart from Fig. 11 present the sum

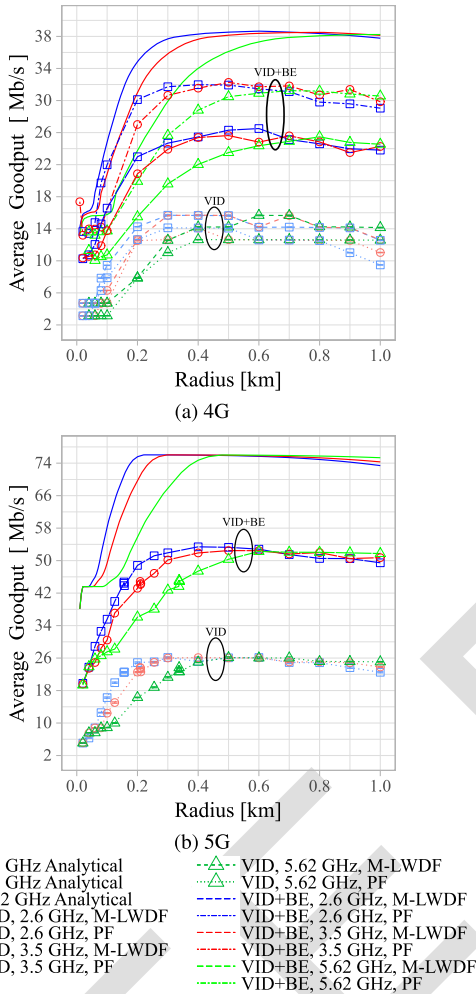


FIGURE 11. 4G and 5G NR maximum average goodput, with either a video (VID) trace 3.1 Mb/s or VID+BE multi-service. The limits of yy axis are different in (a) and (b).

of the goodput of the video and BE flows. For 4G and the PF scheduler, the maximum achievable average goodput was 26.3 Mb/s, 25.6 Mb/s and 25.5 Mb/s for the 2.6 GHz, 3.5 GHz and 5.62 GHz frequency bands and for $R = 500$ m, $R = 500$ m and $R = 800$ m, respectively. For the 5G NR, the maximum average goodput with the video plus the BE has been 53.4 Mb/s, 52.5 Mb/s and 52.2 Mb/s for the 2.6 GHz, 3.5 GHz and 5.62 GHz frequency bands respectively. With VID+BE (compared to VID only), with the PF scheduler, the system capacity is circa 100% higher, after the breakpoint.

As the video application is unable to use all the resources for the $PLR < 2\%$ service quality goal, with the addition of the BE flows, results closer to the analytically supported throughput are achieved for 4G and 5G NR. The considerable difference between the simulated and the analytical results is justified by the use of SINR (instead of EESM) in the analytical modeling.

In 4G, the achieved maximum delay for the PF scheduler, while considering 2.6, 3.5 and 5.62 GHz frequency bands, and $PLR < 2\%$, is 25.7 ms (as shown in Fig. 12), far below

the ITU-T limit of 150 ms for the maximum delay [64]. Although the obtained curves for 5G NR delay are also not presented here, with the PF scheduler, the obtained delay is approximately 15 ms (a decrease of circa 42%).

VII. PERFORMANCE IMPROVEMENT BY USING THE M-LWDF SCHEDULER

This Section presents the comparison between the PF and M-LWDF schedulers through simulation. Only 4G is assumed. The M-LWDF scheduler simultaneously considers delay and QoS and is suitable for RT traffic.

A. PACKET LOSS RATIO

Fig. 13 presents the results for 4G by considering the M-LWDF scheduler. The change in the behavior around the breakpoint distance is similar (compared to the PF). For R_s shorter than d'_{BP}/r_{cc} ($r_{cc} = 3$), in the present study, the average PLR is considerably higher than for R_s longer than the breakpoint distance. It is worthwhile to note that for 4G and the same number of supported users, the M-LWDF clearly presents lower values for the average PLR. As introduced in Section II, the behavior of having much larger values of the PLR for $R \leq d'_{BP}/r_{cc}$ is expected since, somehow, the two-slope behavior penalizes the shortest cell radius.

B. SYSTEM CAPACITY AND DELAY

We have obtained the maximum average goodput and the number of supported users in 4G for the M-LWDF scheduler for a PLR threshold of 2%, as shown in Figs. 11a and 14. The maximum obtained average goodput was ≈ 15.7 Mb/s. The maximum average goodput for the 2.6 GHz frequency band occurs for cell radii in the range from 300 m up to 500 m. At the 3.5 GHz frequency band, the same behavior is observed, but the approximate maximum is obtained between 300 m and 700 m. At 5.62 GHz, the maximum average goodput occurs for R_s between 600 m and 700 m. The average goodput results for the M-LWDF scheduler from Fig. 11a (dashed line) are higher than those obtained with the PF scheduler. For R_s beyond the breakpoint, the resulting system capacity gain compared to PF yields 10-25% and 20-25%, for VID and VID+BE respectively.

The maximum number of supported users is presented in Fig. 14. For both schedulers, the maximum number of supported users has been obtained for values of R longer than the breakpoint distance. For R_s between 20 m and 80 m, the 2.6 GHz and 3.5 GHz frequency bands support the same number of users. For $80 \leq R \leq 250$ m, the best performance occurs for the 2.6 GHz frequency band. Between $250 \leq R \leq 500$ m, the 2.6 GHz and 3.5 GHz frequency bands support the same number of users. R_s beyond 500 m, the 5.62 GHz band presents the best performance. In some cases, the maximum number of users is supported for a larger range of R_s . For the 3.5 GHz frequency band, this behavior occurred for four values of R and three or two times for the 2.6 and 5.62 GHz frequency bands, respectively.

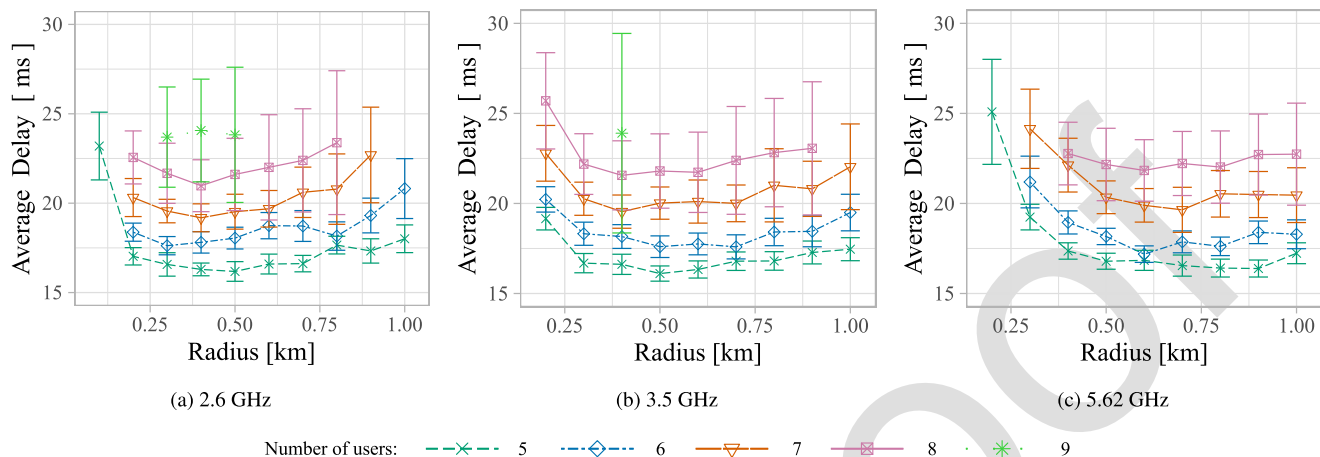


FIGURE 12. 4G PF scheduler maximum average delay with a video trace of 3.1 Mb/s.

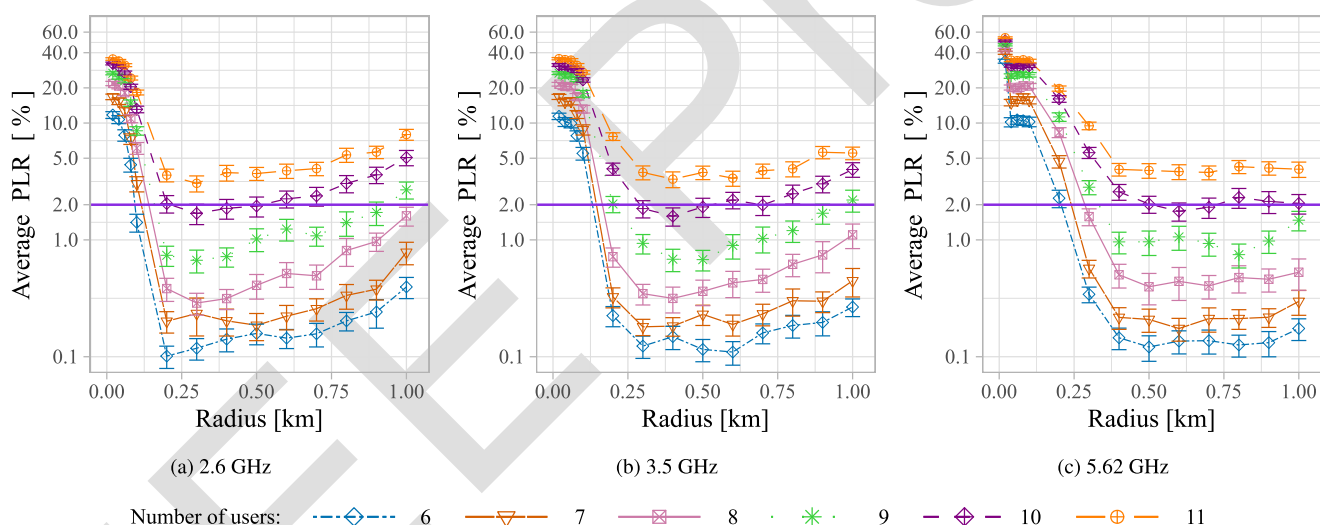


FIGURE 13. 4G results for the average PLR as a function of the cell radius with the number of users as a parameter for the different frequency bands for the M-LWDF scheduler and 3.1 Mb/s video trace.

771 Although view charts for the maximum average delay are
 772 not presented here, from the achieved results, a maximum
 773 average delay of 32 ms occurred for the 3.5 GHz frequency
 774 band for $R = 300$ m and ten supported users. With the M-
 775 LWDF scheduler, although there is an increase in the average
 776 delay, these values are still much lower than the 150 ms
 777 threshold.

778 **VIII. CONCLUSION**

779 This paper investigated the radio resource management
 780 performance of the outdoor sub-6 GHz urban micro cellular
 781 (UMi) scenario considering a dual-slope path loss model
 782 (DS-PLM). The advantages of DS-PLMs in comparison to
 783 single-slope path loss models (SS-PLM) are discussed.

784 The efficiency of 4G and 5G networks in urban outdoor
 785 environments is evaluated using analytical and simulation
 786 results, through the use of the LTE-Sim and 5G-air-simulator

787 environments. The study reveals that, as in the sub-6 GHz
 788 bands, system capacity and performance are constrained
 789 for cell radii shorter than the breakpoint distance, whereas
 790 optimal performance is attained for cell radii longer than
 791 twice the breakpoint distance. It is worthwhile to note that,
 792 by considering various packet schedulers and applications,
 793 the results demonstrate that, even for the same bandwidth, 5G
 794 networks can support more users and attain a higher average
 795 throughput than 4G networks whilst considerably decreasing
 796 the achieved maximum delay, resulting from considering
 797 cyclic prefix orthogonal frequency division multiplexing.
 798 In addition, the inclusion of best effort (BE) flows (modeled
 799 with the infinite-buffer application [40]) can increase the
 800 average goodput of the system.

801 Suggestions for future work include to: i) consider the
 802 EESM/MIESM (not only SINR) in the analysis of the
 803 supported throughput, ii) to include the second ring of

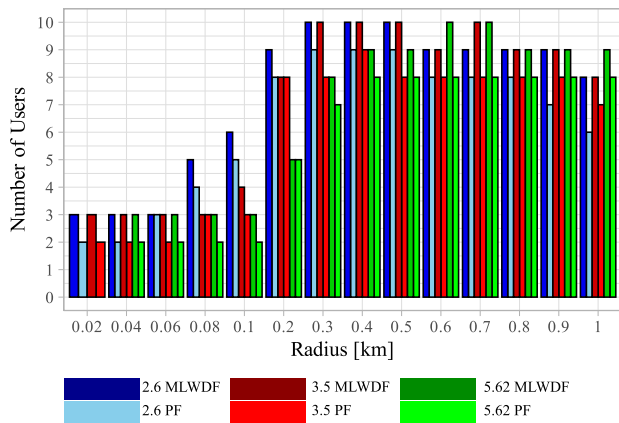


FIGURE 14. 4G maximum number of supported users as a function of the cell radius for different frequency bands.

interference in the system level simulation computations, and iii) further explore the 5G-air-simulator to investigate the M-LWDF in 5G NR and new original packet scheduling schemes or user policies and enhancements in their application to 5G NR, e.g., through the use of reinforcement learning, where exponents of the multiplying factors of the scheduler metric are sought [65].

REFERENCES

- [1] Cisco. (2020). *Cisco Annual Internet Report (2018-2023) White Paper*. Cisco System. [Online]. Available: <https://www.cisco.com/c/en/us/solutions/collateral/executive-perspectives/annual-internet-report/white-paper-c11-741490.pdf>
- [2] Y. Xu and S. Zhou, "On the coverage and capacity of ultra-dense networks with directional transmissions," *IEEE Wireless Commun. Lett.*, vol. 9, no. 3, pp. 271–275, Mar. 2020.
- [3] I. Vila, J. Perez-Romero, O. Sallent, and A. Umberto, "Characterization of radio access network slicing scenarios with 5G QoS provisioning," *IEEE Access*, vol. 8, pp. 51414–51430, 2020.
- [4] H. Munir, S. A. Hassan, H. Pervaiz, Q. Ni, and L. Musavian, "Resource optimization in multi-tier HetNets exploiting multi-slope path loss model," *IEEE Access*, vol. 5, pp. 8714–8726, 2017.
- [5] A. Ghosh, N. Mangalvedhe, R. Ratasuk, B. Mondal, M. Cudak, E. Visotsky, T. A. Thomas, J. G. Andrews, P. Xia, H. S. Jo, H. S. Dhillon, and T. D. Novlan, "Heterogeneous cellular networks: From theory to practice," *IEEE Commun. Mag.*, vol. 50, no. 6, pp. 54–64, Jun. 2012.
- [6] A. Damjanovic, J. Montojo, Y. Wei, T. Ji, T. Luo, M. Vajapeyam, T. Yoo, O. Song, and D. Malladi, "A survey on 3GPP heterogeneous networks," *IEEE Wireless Commun.*, vol. 18, no. 3, pp. 10–21, Jun. 2011.
- [7] S. Q. Gilani, S. A. Hassan, H. Pervaiz, and S. H. Ahmed, "Performance analysis of flexible duplexing-enabled heterogeneous networks exploiting multi slope path loss models," in *Proc. Int. Conf. Comput., Netw. Commun. (ICNC)*, Feb. 2019, pp. 724–728.
- [8] J. Berg, "A recursive method for street microcell path loss calculations," in *Proc. 6th Int. Symp. Pers., Indoor Quality and Mobile Radio Commun.*, vol. 1, Sep. 1995, pp. 140–143.
- [9] N. Garg, S. Singh, and J. Andrews, "Impact of dual slope path loss on user association in HetNets," in *Proc. IEEE Globecom Workshops*, Dec. 2015, pp. 1–6.
- [10] A. Turkmani and A. Arowojolu, "Estimation of signal strength characteristics in typical microcell environments for PCN networks," in *Proc. 2nd IEEE Int. Conf. Universal Pers. Commun.*, Oct. 1993, pp. 69–73.
- [11] H. Munir, S. A. Hassan, H. Pervaiz, Q. Ni, and L. Musavian, "User association in 5G heterogeneous networks exploiting multi-slope path loss model," in *Proc. 2nd Workshop Recent Trends Telecommun. Res. (RTTR)*, Feb. 2017, pp. 1–5.
- [12] U. Demir, C. U. Bas, and S. Coleri Ergen, "Engine compartment UWB channel model for intravehicular wireless sensor networks," *IEEE Trans. Veh. Technol.*, vol. 63, no. 6, pp. 2497–2505, Jul. 2014.
- [13] C. U. Bas and S. C. Ergen, "Ultra-wideband channel model for intravehicular wireless sensor networks," in *Proc. IEEE Wireless Commun. Netw. Conf. (WCNC)*, Apr. 2012, pp. 42–47.
- [14] R. Chen and Z. Zhong, "Analysis on V2V connectivity under dual-slope path loss model in urban scenarios," in *Proc. 30th URSI Gen. Assem. Scientific Symp. (URSI GASS)*, Aug. 2014, pp. 1–4.
- [15] L. Cheng, B. E. Henty, F. Bai, and D. D. Stancil, "Highway and rural propagation channel modeling for vehicle-to-vehicle communications at 5.9 GHz," in *Proc. IEEE Antennas Propag. Soc. Int. Symp.*, Jul. 2008, pp. 1–4.
- [16] I. Rashdan, M. Walter, W. Wang, and G. Cair, "Large scale fading characteristics for vehicle-to-cyclist channel in urban environment at 5 GHz," in *Proc. 14th Eur. Conf. Antennas Propag. (EuCAP)*, Mar. 2020, pp. 1–5.
- [17] R. Chen, Z. Sheng, M. Ni, Z. Zhong, and D. G. Michelson, "Channel capacity under measurement-based model for cooperative vehicular ad hoc networks," in *Proc. IEEE Int. Symp. Antennas Propag. USNC/URSI Nat. Radio Sci. Meeting*, Jul. 2015, pp. 302–303.
- [18] M. G. Doone, S. L. Cotton, D. W. Matolak, C. Oestges, S. F. Heaney, and W. G. Scanlon, "Pedestrian-to-vehicle communications in an urban environment: Channel measurements and modeling," *IEEE Trans. Antennas Propag.*, vol. 67, no. 3, pp. 1790–1803, Mar. 2019.
- [19] P. L. Mehta and R. Prasad, "SINR based capacity performance analysis of hovering ad-hoc network," in *Proc. 19th Int. Symp. Wireless Pers. Multimedia Commun. (WPMC)*, Nov. 2016, pp. 147–152.
- [20] M. F. Abughalia, S. M. Tasmeh Ahsan, and S. Saha, "Comparative study of Microcell's performance using different models in different regions," in *Proc. Int. Conf. Robotics, Electrical Signal Process. Techn. (ICREST)*, Jan. 2019, pp. 517–521.
- [21] J. Lee, M.-D. Kim, J. Liang, J.-J. Park, and B. Park, "Frequency range extension of the ITU-R NLOS path loss models applicable for urban street environments with 28 GHz measurements," in *Proc. 10th Eur. Conf. Antennas Propag. (EuCAP)*, Apr. 2016, pp. 1–5.
- [22] C. B. Andrade and R. P. F. Hoefel, "IEEE 802.11 WLANs: A comparison on indoor coverage models," in *Proc. CCECE*, May 2010, pp. 1–6.
- [23] N. O. Oyie and T. J. O. Afullo, "A comparative study of dual-slope path loss model in various indoor environments at 14 to 22 GHz," in *Proc. Prog. Electromagn. Res. Symp. (PIERS-Toyama)*, Aug. 2018, pp. 121–128.
- [24] S. Sun, T. A. Thomas, T. S. Rappaport, H. Nguyen, I. Z. Kovacs, and I. Rodriguez, "Path loss, shadow fading, and line-of-sight probability models for 5G urban macro-cellular scenarios," in *Proc. IEEE Globecom Workshops (GC Wkshps)*, Dec. 2015, pp. 1–7.
- [25] S. Sousa, F. J. Velez, and J. M. Peha, "Impact of propagation model on capacity in small-cell networks," in *Proc. Int. Symp. Perform. Eval. Comput. Telecommun. Syst. (SPECTS)*, Jul. 2017, pp. 1–8.
- [26] Y. Chang, S. Baek, S. Hur, Y. Mok, and Y. Lee, "A novel dual-slope mm-wave channel model based on 3D ray-tracing in urban environments," in *Proc. IEEE 25th Annu. Int. Symp. Pers., Indoor, Mobile Radio Commun. (PIMRC)*, Sep. 2014, pp. 222–226.
- [27] K. Kitao, T. Imai, N. Tran, N. Omaki, Y. Okumura, M. Inomata, M. Sasaki, and W. Yamada, "Path loss prediction model for 800 MHz to 37 GHz in NLOS microcell environment," in *Proc. IEEE 26th Annu. Int. Symp. Pers., Indoor, Mobile Radio Commun. (PIMRC)*, Aug. 2015, pp. 414–418.
- [28] Y. F. Solahuddin and R. Mardeni, "Indoor empirical path loss prediction model for 2.4 GHz 802.11n network," in *Proc. IEEE Int. Conf. Control Syst., Comput. Eng.*, Nov. 2011, pp. 12–17.
- [29] A. Narayanan, M. I. Rochman, A. Hassan, B. S. Firmansyah, V. Sathya, M. Ghosh, F. Qian, and Z.-L. Zhang, "A comparative measurement study of commercial 5G mmWave deployments," in *Proc. IEEE INFOCOM Conf. Comput. Commun.*, May 2022, pp. 800–809.
- [30] *Further Advancements for E-UTRA Physical Layer Aspects (Release 9)*, document TR 36.814, 3rd Generation Partnership Project, Mar. 2017. [Online]. Available: https://www.3gpp.org/ftp/Specs/archive/36_series/36.814/36814-920.zip
- [31] H. A. M. Ramli, "A study on packet scheduling algorithms for healthcare contents over fifth generation (5G) mobile cellular network," *Int. J. Electron. Telecommun.*, vol. 66, pp. 729–735, Jan. 2020.

- [32] P. Uthansakul, P. Anchuen, M. Uthansakul, and A. A. Khan, "QoE-aware self-tuning of service priority factor for resource allocation optimization in LTE networks," *IEEE Trans. Veh. Technol.*, vol. 69, no. 1, pp. 887–900, Jan. 2020.
- [33] R. R. Paulo and F. J. Velez, "An extensive study on the performance evaluation and scheduling of HeNBs," *IEEE Access*, vol. 9, pp. 40098–40110, 2021.
- [34] E. Skondras, A. Michalas, A. Sgora, and D. D. Vergados, "A downlink scheduler supporting real time services in LTE cellular networks," in *Proc. 6th Int. Conf. Inf., Intell., Syst. Appl. (IISA)*, Jul. 2015, pp. 1–6.
- [35] B. Abdelmula, H. S. Ali, M. Warip, M. N. Bin, O. Bi, and Y. Naimah, "Technical review of RRM for carrier aggregation in LTE-advanced," *J. Theor. Appl. Inf. Technol.*, vol. 91, no. 2, pp. 397–410, Sep. 2016.
- [36] M. M. Nasralla, "A hybrid downlink scheduling approach for multi-traffic classes in LTE wireless systems," *IEEE Access*, vol. 8, pp. 82173–82186, 2020.
- [37] S. Sousa, F. J. Velez, and J. M. Peha, "Impact of considering the ITU-R two slope propagation model in the system capacity trade-off for LTE-A HetNets with small cells," in *Proc. 32nd General Assembly Scientific Symp. Int. Union Radio Science (URSI GASS)*, Aug. 2017, pp. 1–4.
- [38] E. B. Teixeira, A. R. Ramos, M. S. Lourenço, F. J. Velez, and J. M. Peha, "Capacity/cost trade-off for 5G small cell networks in the UHF and SHF bands," in *Proc. 22nd Int. Symp. Wireless Pers. Multimedia Commun. (WPMC)*, Nov. 2019, pp. 1–6.
- [39] E. Teixeira, S. Sousa, F. J. Velez, and J. M. Peha, "Impact of the propagation model on the capacity in small-cell networks: Comparison between the UHF/SHF and the millimeter wavebands," *Radio Sci.*, vol. 56, no. 5, pp. 1–13, May 2021, doi: 10.1029/2020RS007150.
- [40] G. Piro, L. A. Grieco, G. Boggia, F. Capozzi, and P. Camarda, "Simulating LTE cellular systems: An open-source framework," *IEEE Trans. Veh. Technol.*, vol. 60, no. 2, pp. 498–513, Feb. 2011.
- [41] R. R. Paulo and F. J. Velez, "System level simulation of urban microcellular 4G scenarios in the sub-6 GHz frequency bands," in *Proc. Telecoms Conf. (ConfTELE)*, Feb. 2021, pp. 1–6.
- [42] S. Martiradonna, A. Grassi, G. Piro, and G. Boggia, "5G-air-simulator: An open-source tool modeling the 5G air interface," *Comput. Netw.*, vol. 173, May 2020, Art. no. 107151. [Online]. Available: <https://www.sciencedirect.com/science/article/pii/S1389128619317359>
- [43] *Guidelines for Evaluation of Radio Interface Technologies for IMT-Advanced*, document ITU-R M.2135-1, Dec. 2009. [Online]. Available: <https://www.itu.int/pub/R-REP-M.2135-1-2009>
- [44] *Services and Service Capabilities (Release 16)*, document TS 22.105, 3GPP, 2020. [Online]. Available: https://www.3gpp.org/ftp/Specs/archive/22_series/22.105/22105-g00.zip
- [45] X. Zhang and J. G. Andrews, "Downlink cellular network analysis with a dual-slope path loss model," in *Proc. IEEE Int. Conf. Commun. (ICC)*, Jun. 2015, pp. 3975–3980.
- [46] J. Choi, H. Oh, and H. C. Jeon, "Propagation prediction for LTE small cells with antenna beam tilt," in *Proc. IEEE 80th Veh. Technol. Conf.*, Sep. 2014, pp. 1–5.
- [47] A. Merwaday, R. Vannithamby, M. M. Rashid, Y. Zhang, C. Chen, and X. Wu, "On the performance of directional communications in ultra-dense networks," in *Proc. IEEE Int. Conf. Commun. Workshops*, May 2017, pp. 522–527.
- [48] K. Shehzad, N. M. Khan, and J. Ahmed, "Impact of frequency reuse and flexible cell association on the performance of dense heterogeneous cellular networks using dual-slope path loss model," *IEEE Access*, vol. 7, pp. 166214–166234, 2019.
- [49] A. Karttunen, A. F. Molisch, S. Hur, J. Park, and C. J. Zhang, "Spatially consistent street-by-street path loss model for 28-GHz channels in micro cell urban environments," *IEEE Trans. Wireless Commun.*, vol. 16, no. 11, pp. 7538–7550, Nov. 2017.
- [50] *Study on Channel Model for Frequencies From 0.5 To 100 GHz (Release 16)*, document TR 38.901, V16.1.0, 3GPP, 2019. [Online]. Available: https://www.3gpp.org/ftp/Specs/archive/38_series/38.901/38901-g10.zip
- [51] *Guidelines for Evaluation of Radio Interface Technologies for IMT-2020*, document ITU-R M.2412-0, Nov. 2017. [Online]. Available: https://www.itu.int/dms_pub/itu-r/opb/rep/R-REP-M.2412-2017-PDF-E.pdf
- [52] S. Sesia, I. Toufik, and M. Baker, *LTE, The UMTS Long Term Evolution: From Theory to Practice*, 2nd ed. Hoboken, NJ, USA: Wiley, 2011.
- [53] M. Andrews, "Instability of the proportional fair scheduling algorithm for HDR," *IEEE Trans. Wireless Commun.*, vol. 3, no. 5, pp. 1422–1426, Sep. 2004.
- [54] M. I. Rochman, V. Sathya, N. Nunez, D. Fernandez, M. Ghosh, A. S. Ibrahim, and W. Payne, "A comparison study of cellular deployments in Chicago and Miami using apps on smartphones," in *Proc. 15th ACM Workshop Wireless Netw. Testbeds, Experim. Eval. Characterization*. New York, NY, USA: Association for Computing Machinery, Jan. 2022, pp. 61–68, doi: 10.1145/3477086.3480843.
- [55] V. Sathya, M. I. Rochman, and M. Ghosh, "Measurement-based coexistence studies of LAA & Wi-Fi deployments in Chicago," *IEEE Wireless Commun.*, vol. 28, no. 1, pp. 136–143, Feb. 2021.
- [56] R. R. Paulo and F. J. Velez. (2020). *LTE-SIM-ITU-R-M.2135-1*. [Online]. Available: <https://github.com/RRP-IT/LTE-SIM-ITU-R-M.2135-1.git>
- [57] R. R. Paulo and F. J. Velez. (2022). *5G-Air-Simulator_ITU-R-M-2412-0*. [Online]. Available: https://github.com/RRP-IT/5G-air-simulator_ITU-R-M-2412-0.git
- [58] S. Mumtaz and A. Gameiro, "Enhanced algorithm for link to system interface mapping," *Int. J. Comput. Sci. Inf. Secur.*, vol. 3, no. 3, pp. 1–3, Jul. 2009.
- [59] S. Ahmadi, *LTE-Advanced: A Practical Systems Approach to Understanding 3GPP LTE Releases 10 and 11 Radio Access Technologies*, 1st ed. Cambridge, MA, USA: Academic Press, 2013.
- [60] *Feasibility Study for Orthogonal Frequency Division Multiplexing (OFDM) for UTRAN enhancement (Release 6)*, document TR 25.892, V6.0.0, 3GPP, Jun. 2004. [Online]. Available: https://www.3gpp.org/ftp/Specs/archive/25_series/25.892/25892-600.zip
- [61] X. He, K. Niu, Z. He, and J. Lin, "Link layer abstraction in MIMO-OFDM system," in *Proc. Int. Workshop Cross Layer Design*, Sep. 2007, pp. 41–44.
- [62] *Physical Layer Procedures (Release 17)*, TS 36.213, V17.0.0, 3GPP, Dec. 2021. [Online]. Available: https://www.3gpp.org/ftp/Specs/archive/36_series/36.213/36213-h00.zip
- [63] D. Robalo, F. J. Velez, R. R. Paulo, and G. Piro, "Extending the LTE-sim simulator with multi-band scheduling algorithms for carrier aggregation in LTE-advanced scenarios," in *Proc. IEEE 81st Veh. Technol. Conf.*, May 2015, pp. 1–6.
- [64] *Series G: Transmission Systems and Media, Digital Systems and Networks*, document ITU-T Recommendation G.114, May 2003. [Online]. Available: <https://www.itu.int/rec/T-REC-G.114-200305-1/en>
- [65] Q. Zhang, S. Gao, L. Wen, and X.-X. Yang, "Ultra-thin low-cost electronically-beam-scanning reflectarray for Ka-band satellite communications on the move and 6G," in *Proc. Int. Workshop Antenna Technol. (iWAT)*, May 2022, pp. 9–12.



RUI R. PAULO (Member, IEEE) received the Licenciatura and M.Sc. degrees in electromechanical engineering and the Ph.D. degree in electrical and computer engineering from Universidade da Beira Interior (UBI), Covilhã, Portugal, in 2005, 2008, and 2022, respectively. He is currently a Science and Technology Manager with the Instituto de Telecomunicações. He has served as a Volunteer with the VTS Portugal Chapter, since 2006. He has been with the Instituto de Telecomunicações, since 2006. His research interests include teletraffic engineering for wireless communications, radio resource management for small-cell networks, packet scheduling, and network optimization in heterogeneous networks with femtocells.



EMANUEL B. TEIXEIRA (Member, IEEE) received the Licenciatura degree in bioengineering and the M.Sc. degree in electrical and computer engineering from Universidade da Beira Interior (UBI), Covilhã, Portugal, in 2012 and 2014, respectively, where he is currently pursuing the Ph.D. degree in electrical and computer engineering. He has been a Junior Researcher with the Instituto de Telecomunicações, since 2014. His research interests include cellular planning tools, spectrum sharing in small cell networks in millimeter wavebands and cost/revenue performance mobile communication systems, and energy harvesting, biosensors, and image analysis.



FERNANDO J. VELEZ (Senior Member, IEEE) received the Licenciado, M.Sc., and Ph.D. degrees in electrical and computer engineering from the Instituto Superior Técnico, Technical University of Lisbon, in 1993, 1996, and 2001, respectively. Since 1995, he has been with the Department of Electromechanical Engineering, Universidade da Beira Interior, Covilhã, Portugal, where he is currently an Assistant Professor. He is also a Senior Researcher with the Instituto de Telecomunicações. He was an IEF Marie Curie Research Fellow of King's College London—KCL (OPTIMOBILE IEF), from 2008 to 2009 and a Marie Curie ERG Fellow with Universidade da Beira Interior (PLANOPTI ERG), from 2010 to March 2013. He is the Coordinator of the Instituto de Telecomunicações Team, Marie Skłodowska-Curie ITN Action (TeamUp5G), which began, in 2019. He is or was part of the teams of several European and Portuguese research projects on mobile communications. He was the coordinator of six Portuguese projects. Recently, he was the Coordinator of CONQUEST (CMU/ECE/0030/2017), an Exploratory Project from Carnegie Mellon University (CMU), Portugal, a collaboration with the Department of Engineering and Public Policy, CMU. He has authored four books, 25 book chapters, 182 articles and communications in international journals and conferences, and 40 in national conferences. He is an IEEE VTS Region 8 (Europe, Middle East, and Africa) Chapter Coordinator (nominated by VTS in 2010) and was the elected IEEE VTS Portugal Chapter Coordinator, from 2006 to 2014. He is also the Officer of Telecommunications Specialization of Ordem dos Engenheiros. He was the Coordinator of WG2 (on cognitive radio/software-defined radio co-existence studies) of COST IC0905 TERRA. His research interests include cellular planning tools, traffic from mobility, wireless body sensor networks and wearable technologies, cross-layer design, spectrum sharing/aggregation, and cost/revenue performance of advanced mobile communication systems. He is the Co-Chair of the Vertical Team 4 (Smart Cities and Buildings) of COST CA20120 INTERACT.

• • • 1096